Journal of Photochemistry & Photobiology, A: Chemistry 440 (2023) 114658

Contents lists available at ScienceDirect

Journal of Photochemistry & Photobiology, A: Chemistry

journal homepage: www.elsevier.com/locate/jphotochem

Thermal and photochemical reactions of n-pyridinebenzopyrylium multistate of species (n = 2′,3′,4′). Exploring the synthetic potentialities from the unique reactivity of position 2′

Ambrósio Camuenho [a], A. Jorge Parola [a,*], Alfonso Alejo-Armijo [a,1,*], Clara S.B. Gomes [a,b,c], César A.T. Laia [a], Fernando Pina [a]

[a] LAQV-REQUIMTE, Department of Chemistry, FCT-NOVA, NOVA School of Science and Technology, Universidade NOVA de Lisboa, 2829-516 Caparica, Portugal
[b] UCIBIO, Department of Chemistry, FCT-NOVA, NOVA School of Science and Technology, Universidade NOVA de Lisboa, 2829-516 Caparica, Portugal
[c] i4HB, FCT-NOVA, NOVA School of Science and Technology, Universidade NOVA de Lisboa, 2829-516 Caparica, Portugal

ARTICLE INFO

Keywords:
Chromenes
Chalcones
Multistate systems
Photoisomerization
Ring-chain tautomerism

ABSTRACT

The kinetics and thermodynamics of the pH-dependent multistate of species generated by the *trans*-chalcone of n-pyridinebenzopyrylium (n = 2′, 3′) were studied by UV–vis spectroscopy, ^{1}H NMR and HPLC-MS, and the results compared with those reported for n = 4′. Due to the slow kinetics of the multistate species interconversion, the conjugation of these techniques has shown to be a powerful tool to investigate the behaviour of these systems. The species involved in the multistate are *mutatis mutandis* the same observed in anthocyanins and related compounds except for the flavylium cation, which was not observed in these systems even in very acidic medium. The rates of the interconversion of the multistate species upon pH stimuli are much slower than in anthocyanins. The compound bearing the pyridine nitrogen in position 2′ gives two novel products absorbing in the visible. Formation of the new products is particularly efficient from the thermal evolution of the photochemical products obtained upon light irradiation of the protonated *trans*-chalcone in a mixture of methanol:acidic water (1:1). This confirms the unique capacity of the substituents in position 2′ in giving intramolecular reactions involving the benzopyrylium core. Crystal structures for the three pyridine chalcone compounds (n = 2′, 3′, 4′) were obtained and the respective structures discussed.

1. Introduction

Anthocyanins, the molecules responsible for the red to blue colours in most flowers and fruits are labelled by the respective flavylium cation, Scheme 1. [1–5] However, flavylium cation is a sole species, appearing in acidic conditions (pH ≤ 1) of a much more complex chemical system. As shown in Scheme 1, flavylium cation generates a multistate of chemical species (here on designated multistate) reversibly interconnected by external stimuli, such as pH and light.[5,6].

In spite of the complexity of Scheme 1, exhibiting five chemical species interconnected through four different chemical reactions, the multi-equilibrium can be considered as a single acid-base equilibrium between flavylium cation and its conjugate base CB, eq.(1), with an acid-base constant K'_a defined by eq.(3). The conjugated base CB is composed by the neutral species, eq.(2).

$$AH^+ + H_2O \rightleftharpoons CB + H_3O^+ \qquad K'_a \tag{1}$$

$$[CB] = [A] + [B] + [Cc] + [Ct] \tag{2}$$

$$K'_a = K_a + K_h + K_hK_t + K_hK_tK_i \tag{3}$$

At very high proton concentrations the system converges to flavylium cation (red arrows in Scheme 1). Due to its pH dependence and the quite different timescales of the chemical reactions involved, the system is conveniently studied by the so-called direct pH jumps, consisting in the addition of base to equilibrated solutions of the flavylium cation. The relaxation kinetics towards the new equilibrium gives crucial information on the system. Moreover, addition of acid to solutions equilibrated

* Corresponding authors.
E-mail addresses: ajp@fct.unl.pt (A. Jorge Parola), aalejo@ujaen.es (A. Alejo-Armijo).
[1] Present address: Departamento de Química Inorgánica y Orgánica, Facultad de Ciencias Experimentales, Universidad de Jaén, Campus de Excelencia Internacional Agroalimentario, ceiA3, 23071 Jaén, Spain.

https://doi.org/10.1016/j.jphotochem.2023.114658
Received 22 December 2022; Received in revised form 27 February 2023; Accepted 28 February 2023
Available online 4 March 2023

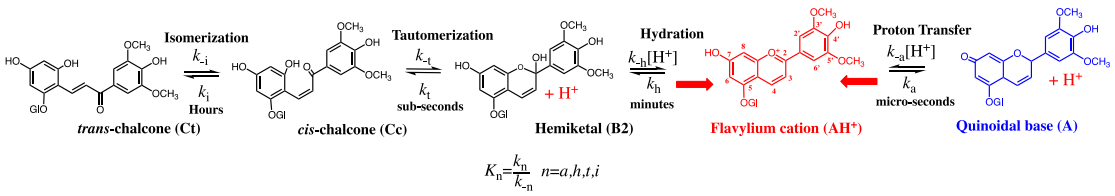

$$K_n = \frac{k_n}{k_{-n}} \quad n = a,h,t,i$$

Scheme 1. The sequence of chemical reactions of flavylium compounds in acidic medium exemplified for malvidin-3-glucoside multistate.[5] At high proton concentrations the system converges to flavylium cation (red arrows). In moderately acidic to basic solutions deprotonated species (not shown) are formed. All reactions take place in very different timescales.

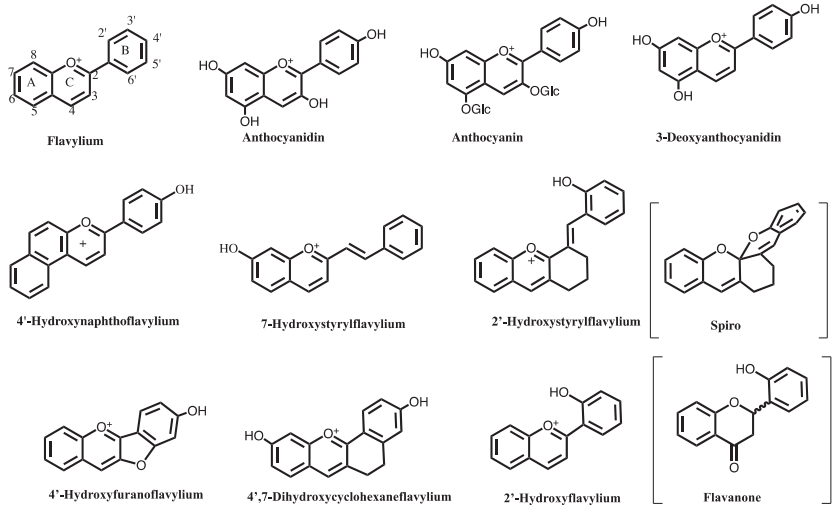

Scheme 2. Examples of compounds exhibiting multistates of species similar to that of anthocyanins; in brackets the new species that are added to the multistate by 2′-hydroxy derivatives.

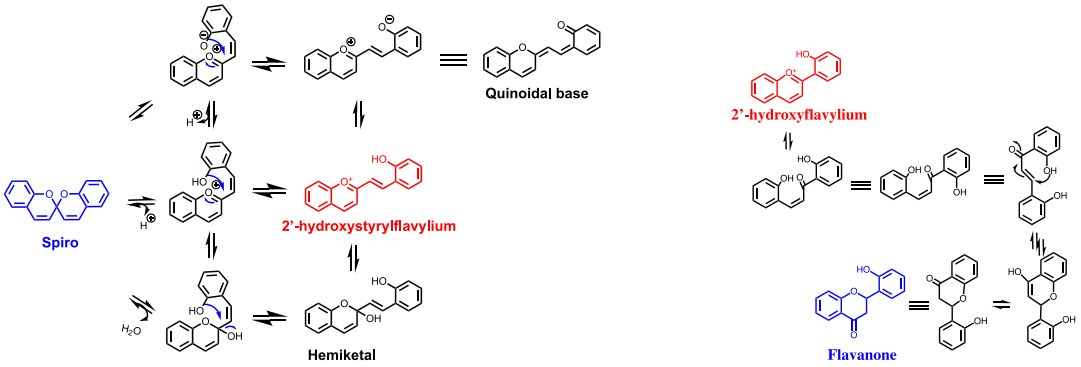

Scheme 3. Formation of spiro (a) and flavanone (b) species in the multistates of 2′-hydroxystyrylflavylium [11,12] and 2′-hydroxyflavylium, [13] respectively.

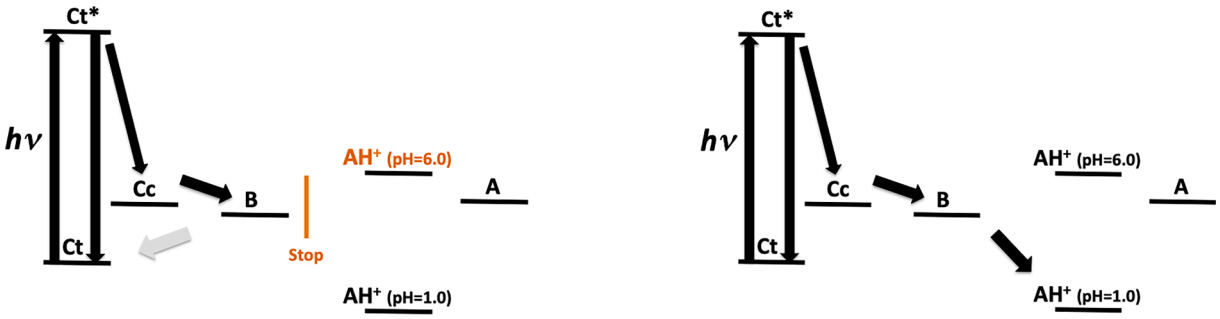

Scheme 4. **(a)** Disappearance (pH = 6.0) or **(b)** appearance (pH = 1.0) of the colour in flavylium multistate of species upon irradiation of the *trans*-chalcone.

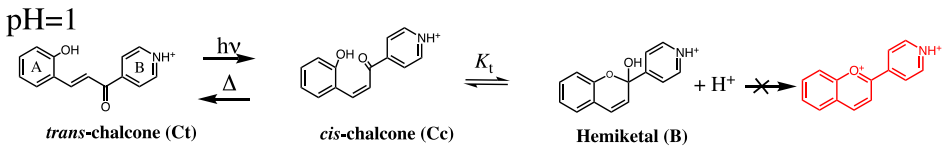

Scheme 5. Photochemistry of Py4. No flavylium cation formation was observed even at very acidic pH values.[12].

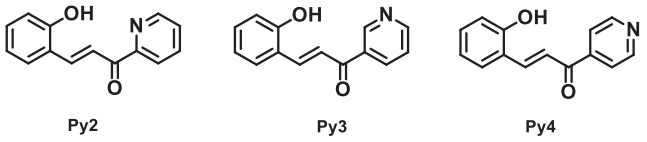

Scheme 6. n-Pyridinechalcones chalcones studied throughout this work. (n = 2′, 3′, 4′).

at higher pH values (reverse pH jumps) complements the information and both procedures combined are generally enough to characterize the system.

Scheme 1 is not exclusive of anthocyanins. There are many natural and synthetic flavylium cations that generate an identical network of reactions like those shown in Scheme 1. In the last years we have shown this ubiquity of the anthocyanins multistate of species in anthocyanidins, 3-deoxyanthocyanidins,[7] furanoflavylium,[8,9] naphthoflavylium, [10] 2′-hydroxystyrylflavylium, [11,12] and 2′-hydroxyflavylium derivarives, [13] Scheme 2.

In some cases, chemical species other than those shown in Scheme 1 can appear in the multistate. This is observed in the multistates generated by 2′-hydroxystyrylflavylium, [11,12] and 2′-hydroxyflavylium, [13] which can form respectively spiro species and flavanones, as exemplified in Schemes 2 and 3.

One interesting property of the multistate of species reported in Scheme 1, is the existence of two sources of potential T-type photochromism: *i)* the *cis–trans* photoisomerization of chalcones[14–18] and the photoinduced ring-opening [16,19,20,21,22] of hemiketals.

In anthocyanins, the mole fraction of *trans*-chalcone at the equilibrium is small and thus photochromism based on the *cis–trans*

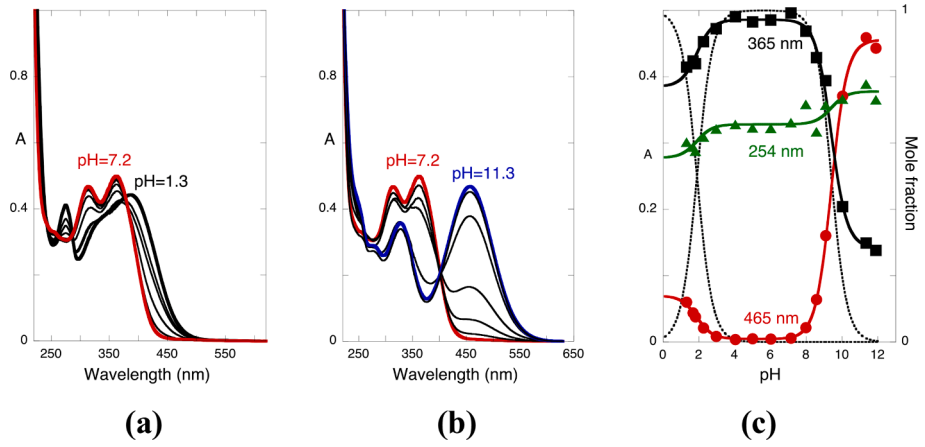

Fig. 1. Spectral variations of freshly prepared solutions of compound **Py2** 1.3×10^{-4} M in water:methanol (1:1) taken immediately after the pH jumps to 1.3 < pH < 7.2 **(a)** and to 7.2 < pH < 11.3 **(b)**, and respective titration curves **(c)**. Fitting was achieved for $pK_{Ct+/Ct} = 1.9$ and $pK_{Ct/Ct-}$=9.4.

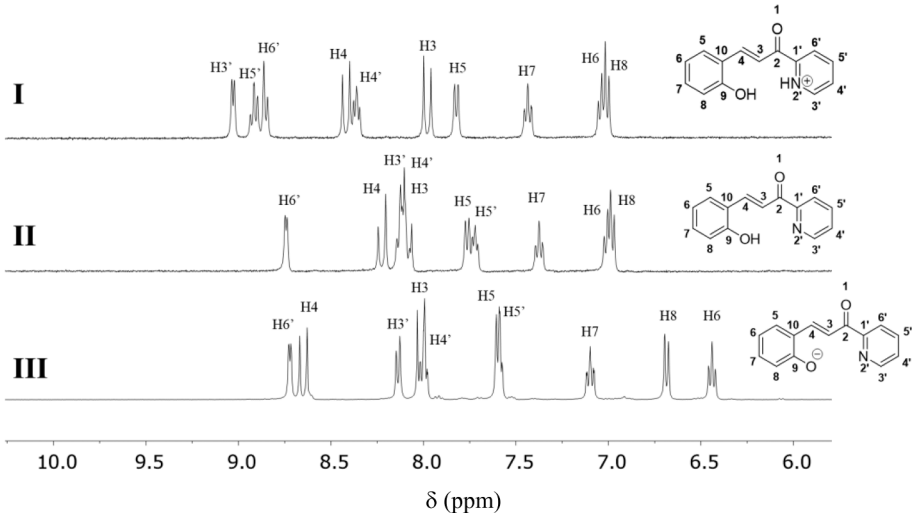

Fig. 2. ^{1}H NMR spectra (400 MHz) of **Py2** 1.7×10^{-3}M in CD_3OD/D_2O (1:1): **I)** pH jump from pD = 6.5 (freshly prepared) to pD = 0.5, 100% Ct^+; **II)** pD = 6.5 (freshly prepared), 100% Ct; **III)** pH jump from pD = 6.5 (freshly prepared) to pD = 12, 100% Ct^-.

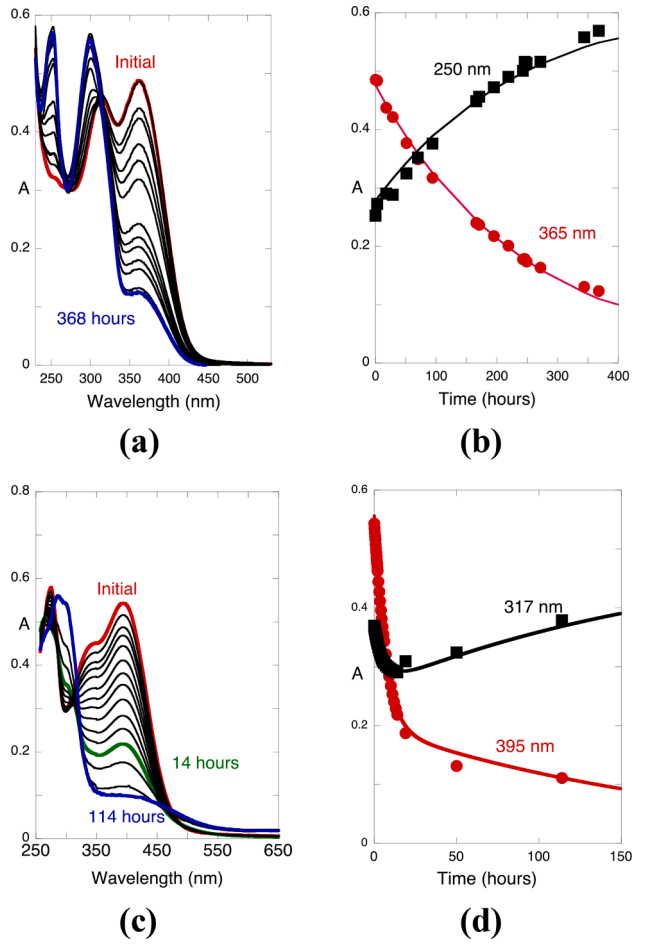

Fig. 3. Spectral variations of a solution of **Py2**, 1.3×10^{-4} M in water:methanol (1:1) at pH = 6.2 **(a)**, and respective kinetic traces fitted with mono-exponential functions with rate constant 1.3×10^{-6} s^{-1} **(b)**; and upon a pH jump from a freshly prepared solution to pH = 1.3 **(c)**. Fitting of the data from (c) was achieved with a bi-exponential law with rate constants 5.0×10^{-5} s^{-1} and 2.3×10^{-5} s^{-1} **(d)**.

isomerization does not have significant expression. [23,24] However, the hemiketal B is the major species and its photoinduced ring opening was reported. [20] Conversely, most synthetic flavylium compounds such as 7-hydroxyflavylium, [25] 4′-hydroxyflavylium [26] and 4′,7-dihydroxyflavylium [14] exhibit *trans*-chalcone (Ct) as the major species. What characterizes the photochromism of these compounds is its dependence on pH. At moderately acidic pH values Ct is the thermodynamic stable species. Upon Ct irradiation, *cis*-chalcone (Cc) is formed and since the *trans* isomer usually possesses higher absorbance, the resulting effect of the irradiation is a decreasing of the colour, followed by the thermal recovery to give back the *trans*-chalcone, Scheme 4a. When there is a high *cis–trans* isomerization barrier it is possible to observe the *trans*-chalcone at pH = 1.0 in a metastable state. Irradiation of the *trans*-chalcone leads to the stable and highly coloured flavylium cation (AH^+) and no recover occurs, Scheme 4b.

A few years ago we reported on a compound possessing a pyridine in position 4′ of ring B, **Py4**, Scheme 5. [27] Irradiation of its Ct species in MeOH:H_2O (1:1) at 365 nm, produces B almost quantitatively through two consecutive photochemical reactions: Ct to Cc photoisomeriaztion followed by Cc to B photo-ring-closure with global quantum yield of 0.02. On the other hand, irradiation of B at 254 nm leads to a photostationary state composed by 80% Ct and 20% B, with quantum yield 0.21.

The lack of flavylium cation in the multisate of **Py4** can be explained by the protonation of the pyridine at pH values where formation of the flavylium cation would be expected. The positive charge in the pyridinium moiety prevents the formation of a 2+ charged species due to the intramolecular electrostatic repulsion. A decrease on the pK'_a values of the systems by 2–3 pH units [28,29] was observed in CTAB micelles, where the positively charged surface of the micelle renders more difficult the formation of the flavylium cation.

Considering the interest of this family of compounds (Scheme 6), in particular their potential photochromic behaviour, we report on the multistates generated by chalcones (**Py2**, **Py3**) that could in theory afford n-pyridinebenzopyrylium (n = 2′,3′) and compare with the previously reported **Py4**. Our main scope is to study the performance of the respective photochromic systems in which regards stability and the effect of the solvent. In particular, by analogy with the reactivity of derivatives with a hydroxyl substituent in position 2′ shown in Scheme 3, we investigate on the possibility of a *mutatis mutandis* intramolecular reaction involving the nitrogen in **Py2**. The slow kinetic processes of the multistates when compared with anthocyanins allowed the use of HPLC/MS conjugated with ^{1}H NMR and UV–vis spectroscopy. This approach has shown to be a powerful tool to study these systems.

2. Experimental

2.1. Materials and methods

Solvents and chemicals employed for synthesis and preparation of samples were of reagent or spectrophotometric grade and used as received; Millipore-grade water was used. Purification by flash chromatography was carried out with Silica gel Carlo Erba 40–60 μm, 60 Å.

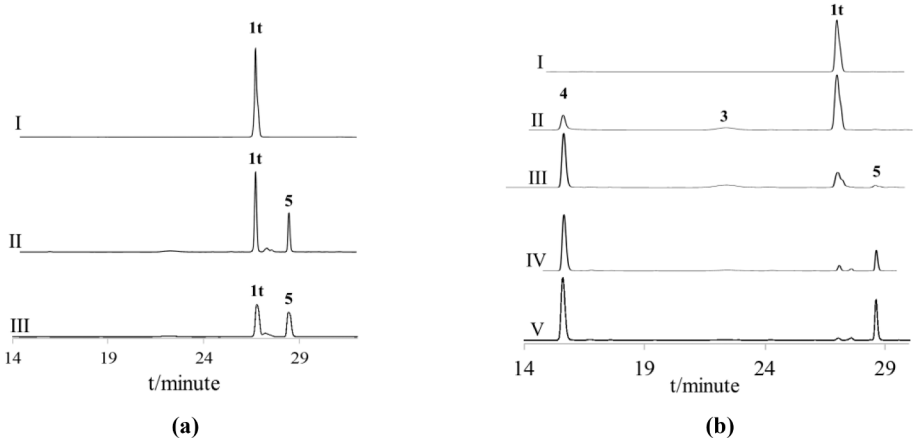

Fig. 4. (a) HPLC chromatograms at 280 nm of **Py2**, 1.1×10^{-4} M in water:methanol (1:1) pH = 6.0: I initial; II after 5 days; III after 7 days. Peaks detected: 1 t (Ct; r.t. = 27.0 min) and peak 5 (r.t. = 28.7 min) which exhibits a *m/z* = 224 (positive mode), see below in scheme 7a the proposed structure for this thermal product; **(b)** the same for 0.48 M in HCl: I initial; II after 6 h; III after 22 h; IV after 5 days; V after 8 days. Peaks detected: Peak 3 (B; r.t. = 22.5 min) (the respective retention time is coincident with a pure hemiketal shown in Fig. 9) and peak 4 (r.t. = 15.7 min) which exhibits a *m/z* = 224 (positive mode), see scheme 7b for the proposed structure.

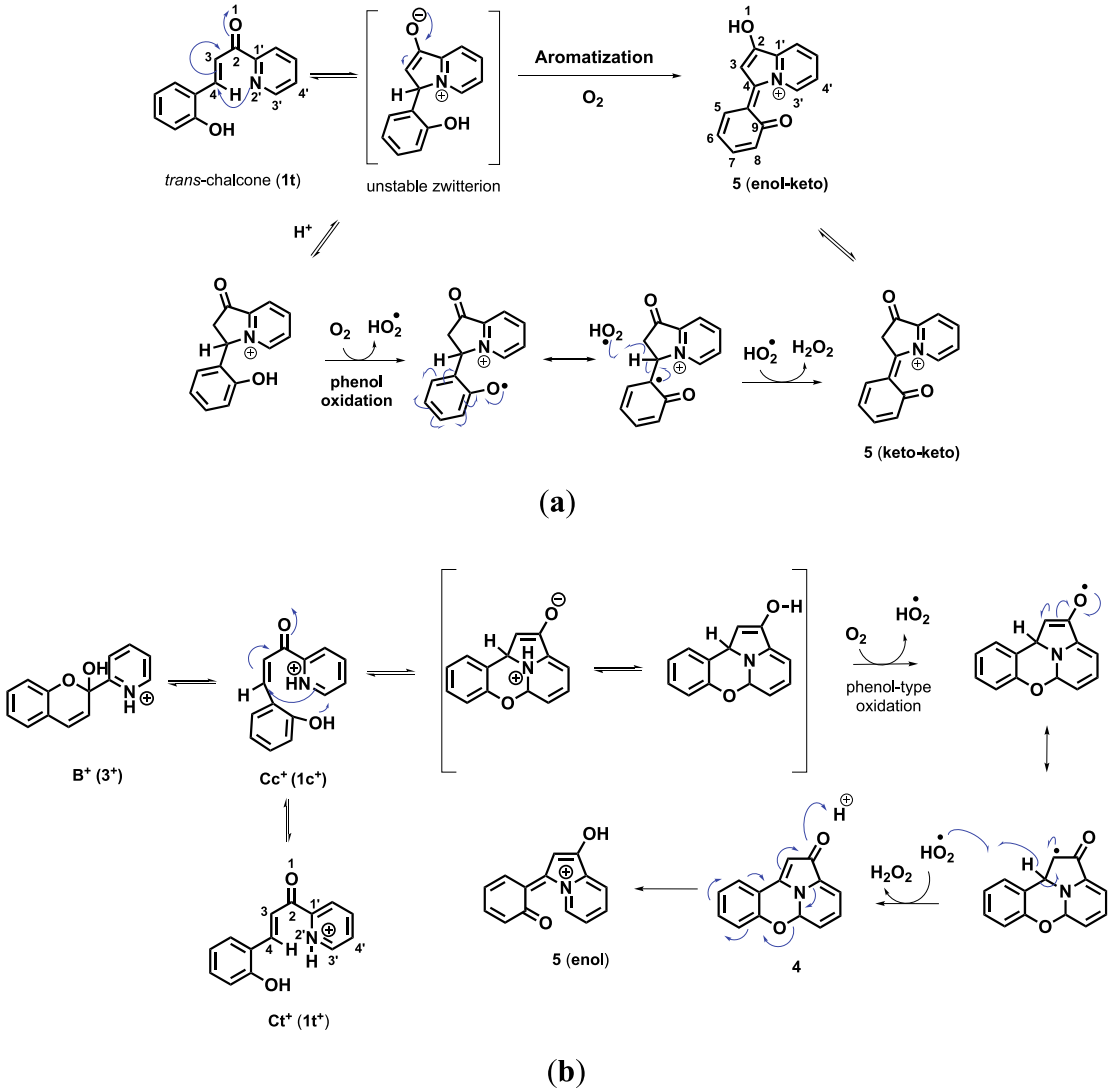

Scheme 7. (**a**) Mechanistic proposal of the formation of compound **5** in neutral conditions. We propose that compound **5** is formed in two steps: (*i*) Michael addition of the nitrogen atom of pyridine chalcone to C-4; (*ii*) oxidation. (**b**) Mechanistic proposal of the formation of compound **5** in acidic conditions. We propose that compound **5** is formed in four steps: (*i*) *cis–trans* isomerization and tautomerization; (*ii*) double nucleophilic ciclyzation by addition of the hydroxyl group to C-3́ and subsequent Michael addition of the nitrogen atom of pyridine to C-4; (*iii*) oxidation (compound **4**) and (*iv*) rearomatization of the pyridine ring (compound **5**).

NMR spectra were run on a Bruker Advance III 400 spectrometer (400 MHz for ^{1}H, 100 MHz for ^{13}C) at 298 K. NMR assignments have been carried out on the basis of 1D (^{1}H, ^{13}C) and 2D (COSY, HSQC and HMBC) NMR spectra. High-performance liquid chromatography (HPLC) analysis was conducted on a Merck-Hitachi instrument equipped with a diode array detector (DAD), scan range: 200–800 nm (Merck-Hitachi L-4500 Diode Array Detector) and operating at 25 °C. Analytical HPLC analyses were performed by a reverse-phase analytical column (RP-HPLC, Purosphere® Star column, 250 mm × 3 mm i.d., 5 μm). Samples were prepared in MeOH and the injection volume was 20 μL. The best peak separation was obtained with H_2O:$HClO_4$, 99.7:0.3, v/v (solvent A) and pure MeOH (solvent B) at a flow rate of 1 mL/min: 7% B for 2 min; linear gradient from 7% to 15% B for 6 min; linear gradient from 15% to 75% B for 17 min; linear gradient from 75% to 80% B for 2 min; linear gradient from 80% to 100% B for another 2 min; 100% B for 11 min and 5 min to return to the initial condition. The total run time excluding equilibration was 40 min. Semipreparative HPLC was conducted on a reverse-phase analytical column (Phenomenex® Onyx Monolithic C18, 100 mm × 10 mm). Samples were prepared in MeOH and the injection volume was 200 μL. The best peak separation was obtained with H_2O: $HClO_4$, 99.7:0.3, v/v (solvent A) and pure MeOH (solvent B) at a flow rate of 4 mL/min using the same elution gradient described before. HPLC/MS analyses were performed in an Agilent 1200 Series equipment coupled with an Agilent 6130B Single Quadrupole detector with API-ES source. Elemental analyses were performed using a Thermofinnigan Flash EA 1112 Series instrument with an error of ± 0.4%. Mass spectra were obtained on an Orbitrap XLTM LTL (ESI-MS) controlled by LTQ Tune Plus 2.5.5 and Xcalibur 2.1.0.

2.2. Thermodynamic and kinetic studies

The pH jumps were carried out by adding a stock solution of *trans*-chalcone (**Py2** or **Py3**, 1 mL) in methanol:water 1:1 at pH 5.9 (**Py2**) or 6.5 (**Py3**) to a 3 mL quartz cuvette containing methanol (1 mL) and universal buffer of Theorell and Stenhagen [30] (1 mL) at the desired final pH. The final pH of the solutions was measured in a Crison basic 20 + pH meter. Spectroscopic measurements were performed using Milli-Q water with a constant temperature of 20 ± 1 °C, with a Varian-Cary 100 Bio spectrophotometer.

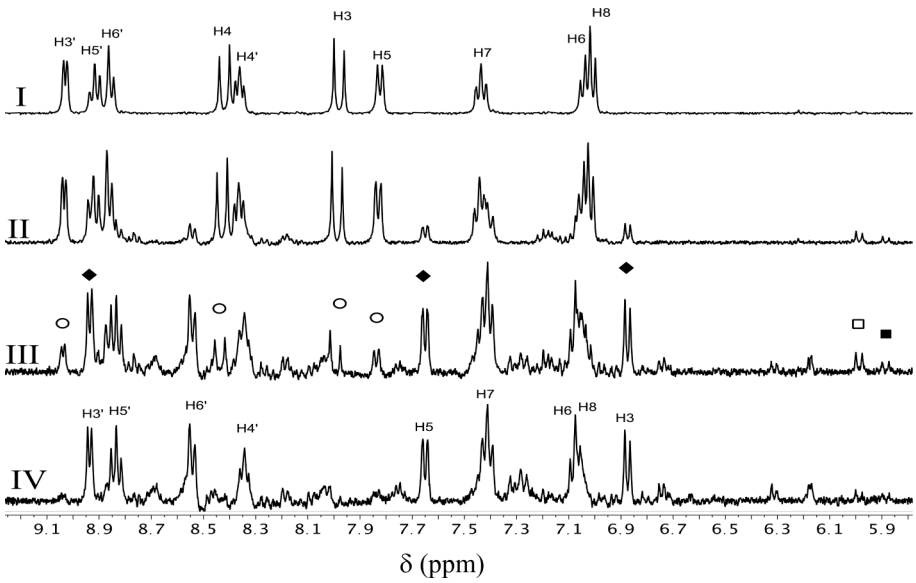

Fig. 5. ^{1}H NMR spectra of **Py2** (1.7×10^{-2}M in CD_3OD:D_2O (1:1), 0.48 M DCl): I) initial; II) 7 h; III) 30 h; IV) 54 h; representative compounds: $\mathbf{3}^{+}$ (B^{+}(■)), $\mathbf{1c}^{+}$ (Cc^{+} (□)), $\mathbf{1t}^{+}$ (Ct^{+} (○)) and $\mathbf{4}^{+}$ (peak 4 (◆)).

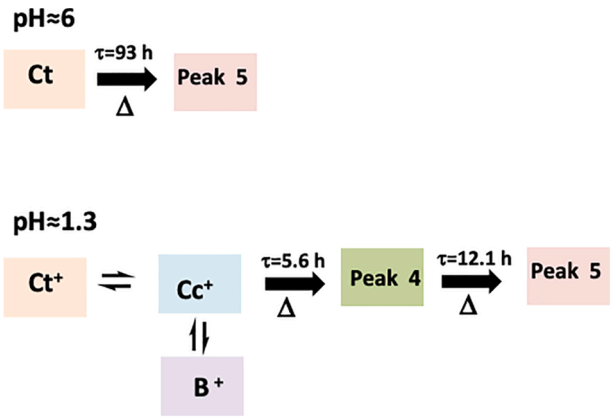

Scheme 8. Summary of the thermal behaviour of **1t** in methanol:water (1:1) mixtures.

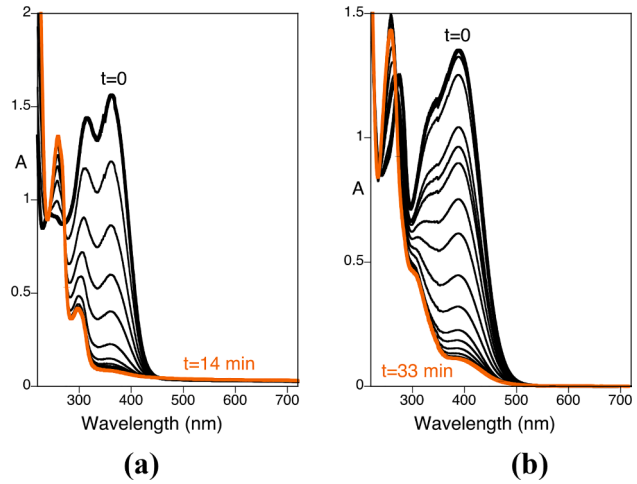

Fig. 6. Spectral variations of freshly prepared solutions of compound **Py2** 1.1×10^{-4} M in water:methanol (1:1) upon irradiation at 365 nm. **(a)** at pH = 6.5; **(b)** at pH = 1.3.

2.3. Photochemical studies

Photochemical studies were carried with irradiation at 365 nm, following by NMR and UV–Vis. *Trans*-chalcone (**Py2** or **Py3**) solutions with concentrations of 1.7×10^{-2} M and 4.0×10^{-5} M in MeOH or MeOH/H_2O (1: 1 v/v) mixtures were prepared for NMR and UV–Vis, respectively. The irradiations were made in quartz cuvettes of 3 mL with 1 cm of optical path. The solutions were irradiated at 365 nm with a 200 W xenon and mercury lamp, controlled by a Newport 69,907 unit, and using a Semrock-MaxLampTM bandpass filter to isolate the 365 nm wavelength, until the photostationary state was reached. The thermodynamic recovery in the dark was followed by NMR and UV–Vis.

2.4. Synthesis

2.4.1. Synthesis of (E)-3-(2-hydroxyphenyl)-1-(pyridin-2-yl)prop-2-en-1-one (Py2)

The synthesis of compound **Py2** was achieved according to the experimental procedure previously described by us [31]. A solution of 1.1 mL of 2-acetylpyridine (10 mmol) and 1 mL of salicylaldehyde (10 mmol) in 15 mL of ethanol was degassed. Then, 1 mL of an aqueous solution of KOH (1 g mL^{-1}) was added dropwise at room temperature, under nitrogen. The reaction mixture was degassed again and stirred at room temperature overnight under inert atmosphere. The solution was neutralized and concentrated under reduced pressure to give a crude residue, which was first purified by flash column chromatography (DCM:Et_2O, 8:2, v/v) and then recrystallized in warm MeOH to give green crystals (0.788 g, 3.5 mmol, 35%). ^{1}H NMR (400 MHz, MeOD-d_4) δ 8.76 (ov, 1H, H-6′), 8.29 (*t*, J = 16 Hz, 2H, H-3 and H-4), 8.16 (*d*, J = 7.8, 1H, 1H, H-3′), 8.01 (*td*, J = 7.7 Hz, 1H, H-4′), 7.72 (ov, 1H, H-5), 7.62 (*ddd*, J = 7.6 Hz, 1H, H-5′), 7.28 (*td*, J = 7.8 Hz, 1H, H-7), 6.91 (*dd*, J = 8.1, 6.7 Hz, 1H, H-6 and H-8); ^{13}C NMR (100 MHz, MeOD-d_4) δ 190.1 (C-2), 157.6 (C-9), 154.3 (C-1′), 148.7 (C-6′), 140.8 (C-4), 137.3 (C-4′), 131.8 (C-7), 128.6 (C-5), 127.0 (C-5′), 122.5 (C-3′), 121.9 (C-10), 119.9 (C-3), 119.5 (C-6), 115.7 (C-8). MS (ESI-MS, positive mode): *m/z* calculated for $[M + H]^{+}$ 226.08; found $[C_{14}H_{12}NO_2]^{+}$ 226.1. EA calculated for $C_{14}H_{11}NO_2$: % C 74.65; % H 4.92; % N 6.22; found: % C 74.46, % H 5.09, % N 6.19.

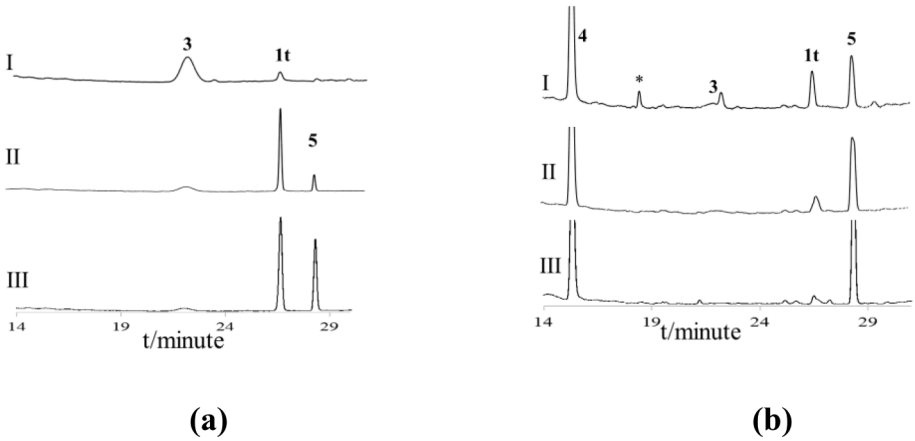

Fig. 7. HPLC chromatograms at 280 nm regarding the dark thermal recovery after irradiation of **1t** at 365 nm; **(a)** (1×10^{-4}M in MeOH/H_2O (1:1), pH = 6, **I** photostationary state reached after 15 min irradiation; **II** the same of **I** after 2 days of dark thermal recovery; **III** the same of **I** after 6 days of dark thermal recovery; peaks detected: **1t** (Ct, r.t. = 27.0 min); **3** (B, r.t. = 22.5 min) and **5** (r.t. = 28.7 min) **(b)** HPLC chromatograms at 280 nm (1×10^{-4}M in MeOH/H_2O (1:1), 0.48 M HCl),: **I**, after 15 min irradiation; **II** the same of **I** after 2 days of dark thermal recovery; **III** the same of **I** after 6 days of dark thermal recovery; peaks detected: **1t** (Ct, r.t. = 27.0 min); **3** (B, r.t. = 22.5 min), **4** (r.t. = 15.7 min) and **5** (r.t. = 28.7 min); *no identified peak.

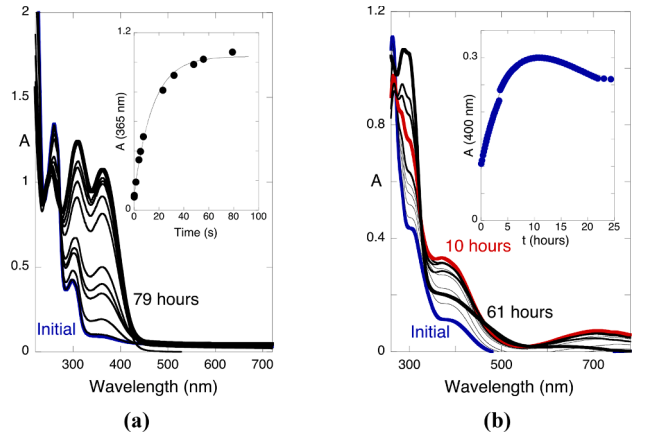

Fig. 8. (a) Thermal recovery of the photochemical products obtained at pH = 6.5 upon irradiation at 365 nm (Fig. 6a). Fitting of the Ct recovery was achieved with a mono-exponential law with rate constant 1.9×10^{-5} s^{-1}. **(b)** The same at pH = 1.3 upon the irradiation experiment reported in Fig. 6b. Fitting was achieved for a bi-exponential process with rate constants 6.0×10^{-5} s^{-1} and 1.3×10^{-5} s^{-1}.

2.4.2. Synthesis of (E)-3-(2-hydroxyphenyl)-1-(pyridin-3-yl)prop-2-en-1-one (Py3)

The synthesis of compound **Py3** was achieved according to the experimental procedure previously described by us. [31] A solution of 0.5 mL of 3-acetylpyridine (4.5 mmol) and 0.45 mL of salicylaldehyde (4.5 mmol) in 7.5 mL of ethanol was degassed. Then, 0.5 mL of an aqueous solution of KOH (1 g mL^{-1}) was added dropwise at room temperature, under nitrogen. The reaction mixture was degassed again and stirred at room temperature overnight under inert atmosphere. The solution was neutralized and concentrated under reduced pressure to give a crude residue, which was first purified by flash column chromatography (DCM:Et_2O, 8:2, v/v) and then recrystallized in warm MeOH: Et_2O (2:1, v/v) to give green crystals (0.48 g, 2.11 mmol, 47%). ^{1}H NMR (400 MHz, MeOD-d_4) δ 9.19 (*s, J* = 2.3 Hz, 1H, H-2′), 8.77 (*dd, J* = 4.9, 1.7 Hz, 1H, H-6′), 8.46 (*dt, J* = 8.0, 2.0 Hz, 1H, H-4′), 8.18 (*d, J* = 15.8 Hz, 1H, H-4), 7.81 (*d, J* = 15.7 Hz, 1H, H-3), 7.72 (*dd, J* = 8.0, 1.7 Hz, 1H, H-5), 7.63 (*dd, J* = 8.0, 4.9 Hz, 1H, H-5′), 7.28 (*dd, J* = 7.8, 1.7 Hz, 1H, H-7), 6.92 (*t, J* = 7.7 Hz, 2H, H-8 and H-6). ^{13}C NMR (100 MHz, MeOD-d_4) δ = 189.80 (C-2), 157.72 (C-9), 152.03 (C-6′), 148.80 (C-2′), 142.23 (C-4), 136.42 (C-4′), 134.16 (C-1′), 132.08 (C-7), 129.26 (C-5), 124.00 (C-5′), 121.45 (C-10), 120.66 (C-3), 119.51 (C-6), 115.75 (C-8). MS (ESI-MS, positive mode): *m/z* calculated for $[M + H]^+$ 226.08; found $[C_{14}H_{12}NO_2]^+$ 226.1. EA calculated for $C_{14}H_{11}NO_2$: %C 74.6; %H 4.6; % N 6.2; found: %C 74.75, %H 5.40, %N 6.21.

2.4.3. Synthesis of (Z)-1-hydroxy-3-(6-oxocyclohexa-2,4-dien-1-ylidene)–3H-indolizin-4-ium (5)

Compound **1** (33 mg, 0.146 mmol) was dissolved in 50 mL of methanol and then 50 mL of aqueous solution of 0.2 M HCl was added dropwise at room temperature. The reaction was monitored by HPLC. After 60 days, compound **5** is the major compound and was purified by semipreparative HPLC yielding compound **5** as a white powder (10 mg; 0.045 mmol, 31%). ^{1}H NMR (400 MHz, MeOD-d_4) δ 8.87 (br *d, J* = 5.7 Hz, 1H), 8.67 (*ov*, 1H), 8.65 (*ov*, 1H), 8.19 (*ov*, 1H), 8.17 (br *d, J* = 8.2

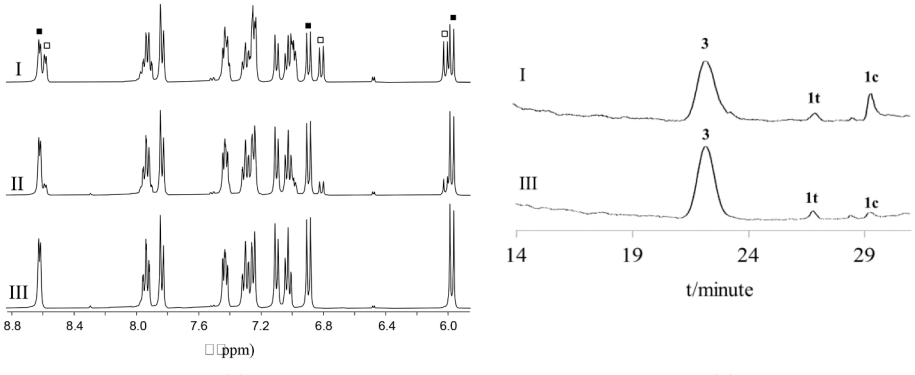

Fig. 9. (a) ^{1}H NMR in CD_3OD. **I** - Compound **Py2**, 1.7×10^{-3} M, after 90 min irradiation at 365 nm; **II** - the same of **I** after 90 min in the dark; **III** - the same of **I** after 20 h in the dark; (■) hemiketal; (□) *cis*-chalcone; **(b)** HPLC chromatograms at 280 nm of the solutions **I** and **III**; peaks detected: **1t** (Ct, r.t. = 27.0 min); **1c** (Cc, r.t. = 29.1 min) and **3** (B, r.t. = 22.5 min).

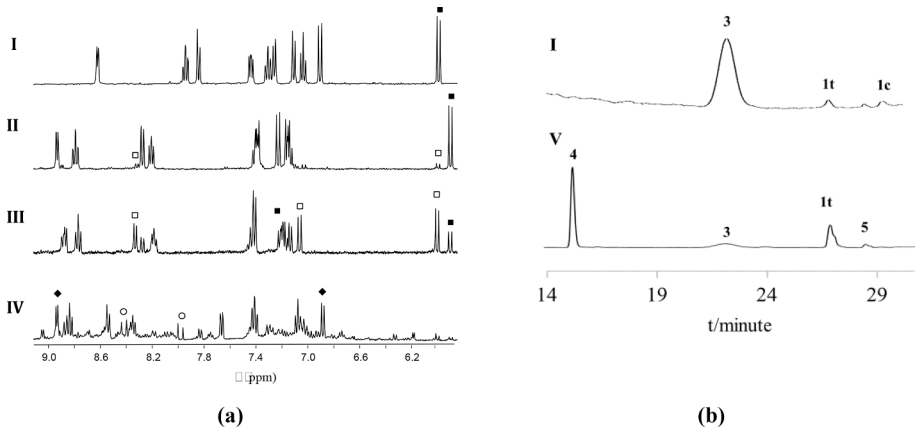

Fig. 10. **(a) I** ^{1}H NMR spectrum of **Py2** (1.7×10^{-2} M) in CD_3OD after 90 min irradiation at 365 nm and 20 h of dark thermal recovery (compound **3**); **II** the same of **I** after addition of 20 μL of DCl (12 M). This solutions does not change after 5 days (mixture of $\mathbf{3}^{+}$ and $\mathbf{1c}^{+}$); **III** the same of **II** after addition of D_2O (final 1:1 *d*-methanol:water); **IV** the same of **III** after 48 h in the dark; (■) hemiketal ($\mathbf{3}^{+}$ and **3**); (□) *cis*-chalcone ($\mathbf{1c}^{+}$ and **1c**); (◆) compound **4**. **b)** HPLC chromatograms at 280 nm (1.7×10^{-3} M, MeOD): **I)** solution **I; V)** solution **III** after 85 h of dark equilibration. Peak detected: peak **1t** (Ct, r.t. = 27.0 min); **1c** (Cc, r.t. = 29.1 min), **3** (B, r.t. = 22.5 min), **4** (r.t. = 15.7 min) and **5** (r.t. = 28.7 min).

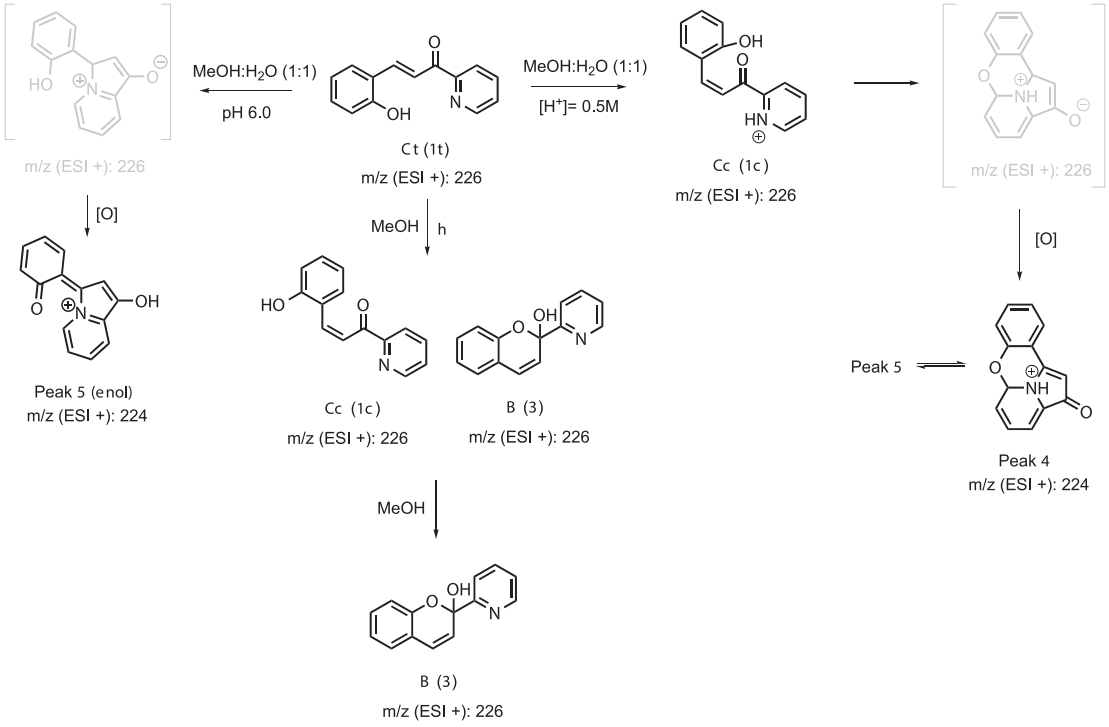

Scheme 9. Summary of behaviour of **1t** in pure methanol and methanol:water (1:1) mixtures.

Hz, 1H), 8.01 (*t*, $J = 8.0$ Hz, 1H), 7.94 (br *d*, $J = 8.7$ Hz, 1H), 7.70 (*ov*, 1H), 7.61 (*s*, 1H). ^{13}C NMR (100 MHz, MeOD-d_4) δ 180.8, 157.3, 157.1, 148.6, 143.7, 140.3, 139.4, 130.8, 128.8, 127.0, 125.3, 120.1, 119.0, 108.7. HPLC-MS (ESI-MS, positive mode): *m/z* calculated for $[M + H]^+$ 224.06; found $[C_{14}H_{10}NO_2]^+$ 224.1.

2.5. Single-crystal X-ray diffraction

The most relevant crystallographic data for each compound and experimental details are presented in Table 2. Crystals suitable for single-crystal X-ray analysis of compounds **Py2**, **Py3** and **Py4** were selected and covered with Fomblin (polyfluoro ether oil) and mounted on a nylon loop. The data was collected at room temperature on a Bruker D8 Venture diffractometer equipped with a Photon 100 detector, using graphite monochromated Mo-Kα or Cu-Kα radiation (λ = 0.71073 Å or λ = 1.5418 Å, respectively). The data was processed using the APEX3 suite software package, which includes integration and scaling (SAINT), absorption corrections (SADABS) and space group determination (XPREP). Structure solution and refinement were done using direct methods with the programs SHELXT 2014/5 and SHELXL (version 2018/3) [32–34] inbuilt in APEX and WinGX-Version 2018.3 [35] software packages. All non-hydrogen atoms were refined anisotropically. Except for the OH in **Py3**, all hydrogen atoms were inserted in idealized positions, and allowed to refine riding on the parent carbon atom with C–H distances of 0.93 Å for aromatic H atoms and O–H distances of 0.82 Å. The molecular diagrams were drawn with ORTEP-3 (version 2014.1) [35,18] and Mercury [36] included in the software package. The data were deposited in CCDC under the deposit numbers 2,207,218 for **Py2**, 2,207,219 for

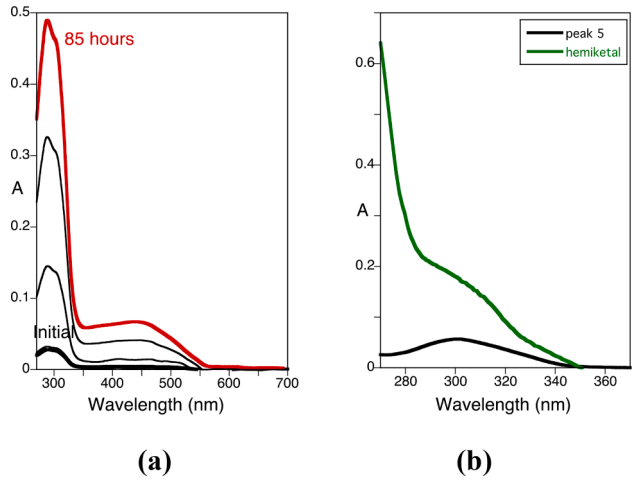

Fig. 11. (a) Absorption spectra of **Py2** (4×10^{-3} M) in methanol:water (1:1) 0.48 M in HCl. Initial spectrum (black) taken upon 2 h irradiation at 365 nm (hemiketal, compound **3**) and its evolution in the dark up to 85 h (red spectrum, compound **4**); **(b)** Absorption spectra of hemiketal and compound **5** from the same experiment.

Py3 and 2,207,220 for **Py4**.

3. Results and discussion

3.1. Multistate of species of *Py2*

3.1.1. Thermal evolution (water:methanol (1:1))

The pH-dependent absorption spectra of freshly prepared[2] Ct solutions of **Py2** taken immediately after the pH jumps are shown in Fig. 1. The spectral variations are compatible with the existence of two pK_as. According to the structure of the molecule the three species are Ct^+, Ct and Ct^-. In Fig. 1a the equilibrium between **Py2** protonated at the pyridine and the neutral form shows a clear isosbestic point. An identical behaviour occurs in Fig. 1b for the equilibrium involving the neutral and the anionic forms. Fitting of the absorbance as a function of pH at three representative wavelengths allows to calculate $pK_{Ct+/Ct} = 1.9$ and $pK_{Ct/Ct-}$=9.4, Fig. 1c.

The results of Fig. 1 were corroborated by ^{1}H NMR data, Fig. 2. Representative pD values were selected on the basis of the UV–vis absorption spectroscopy data shown in Fig. 1. The ^{1}H NMR spectra upon direct pH jumps from freshly prepared solutions at pH = 6.5 containing 100% Ct is shown in Fig. 2. The ^{1}H NMR spectra correspond to the *trans*-chalcones in the cationic (Fig. 2-I), neutral (Fig. 2-II) and anionic forms (Fig. 2-III). The identification of the *trans* isomer in the three cases was achieved through the characteristic large coupling constants between protons 3 and 4 of the chalcone's exo double bond, which are respectively a) 15.6 Hz; b) 16.2 Hz; c) 16.6 Hz.

The thermal evolution of the *trans*-chalcone forms Ct^+ and Ct was monitored by UV–vis absorption, at pH = 6.2, Fig. 3a, and pH = 1.3, Fig. 3b, respectively.

The spectral variations reported in Fig. 3 indicate that the *trans*-chalcone disappears at pH = 6.2 and 1.3 respectively with a mono-exponential law with rate constant 1.3×10^{-6} s^{-1}, and a bi-exponential law with rate constants 5.0×10^{-5} s^{-1} and 2.3×10^{-5} s^{-1}. In order to get more insight on this system, HPLC was used to monitor changes over time, in water:methanol (1:1) at pH = 6.0 and in acidic solutions 0.48 M HCl, Fig. 4.

Inspection of Fig. 4 confirms that *trans*-chalcone form of **Py2** (**1t**) is not stable in solvent mixtures of water:methanol (1:1), neither around neutral nor in very acidic solutions. This behaviour contrasts with the one observed for **Py3** (see Appendix) and **Py4** [12] and is a consequence of the peculiarity of the nitrogen in position 2. The evolution of the *trans*-chalcone at pH = 6.0 is relatively clean and the final product (compound **5**) exhibits a $m/z = 224$ (positive mode).[3] A proposed structure for this thermal product is shown in Scheme 7.

At neutral pH values (Fig. 4a), Ct (**1t**, $m/z = 226$ (positive mode)) is in its neutral form and as a result, the lone pair of the nitrogen atom at the pyridine ring is available to act as a nucleophile to attack intramolecularly the electrophilic double bond (position 4 in scheme 7a). The unstable zwitterion formed (not detected by HPLC nor MS) is rapidly oxidized in order to recover the aromaticity of the system, leading to the stable compound **5** ($m/z = 224$ (positive mode)). At acidic pH values (Fig. 4b), the nitrogen atom of pyridine is protonated and in no longer nucleophilic. However, compound **5** is also produced as the thermodynamic product but its formation is achieved by a different pathway in which compound **4** plays a vital role (Scheme 7b). In this case, protonation of the nitrogen atom at the pyridine enhances the electrophilicity at C-3′ that may be attacked by the phenolic oxygen atom in the protonated *cis*-chalcone species (Cc^+), formed upon isomerization of the protonated *trans*-chalcone (Ct^+). This nucleophilic attack promotes the Michael addition of the nitrogen atom to C-4 in a concerted step, leading to the formation of an unstable intermediate (not detected) which is rapidly oxidized to produce compound **4** ($m/z = 224$ (positive mode)). The last step is a ring opening reaction in order to recover the aromatization at the pyridine ring which allows the formation of compound **5**.

More information regarding the thermal evolution of the *trans*-chalcone **1t** could be achieved after a direct pH jump from freshly prepared solutions of **Py2** in CD_3OD:D_2O (1:1) to pD = 0.5, monitored by ^{1}H NMR, Fig. 5.

The data from Fig. 5 corroborates the HPLC experiments. The formation of B^+ and Cc^+ maintaining the same ratio could be observed which is an indication that the tautomerization is the faster kinetic step and these two species can be considered at equilibrium during all the other kinetic processes. After 7 h (Fig. 5-II), compound **4** starts to appear. It is possible to conclude that this compound is formed from the B^+/Cc^+ in equilibrium and after 54 h (Fig. 5-IV) it is the major product in solution. The formation of compound **5** from compound **4** is much slower (as shown in Fig. 4b) and several days are needed to observe the presence of this compound. In fact, compound **5** could be isolated by semipreparative HPLC (see experimental section) from a two-month aged solution of **1t** in methanol:water (0.2 M HCl) (1:1) and was fully characterized by NMR and MS. ^{1}H NMR shows 9 aromatic signals grouped into three systems: two A_2B_2 systems and one isolated singlet at 7.42 ppm assigned to H-3 (see supporting information). ^{13}C NMR also shows 14 signals, 9 CH aromatic and 5 quaternary signals among which we can highlight the signal at 180.8 ppm assigned to a keto group. The HMBC spectrum allowed to assign the position of the keto group at C-9 due to its correlation with the A_2B_2 aromatic signals at low field. The other A_2B_2 aromatic signals at higher field were assigned to the pyridine ring system which correlated with the signal at 140.3 ppm associated with the enolic carbon at C-2 (see supporting information for a complete assignment).

As a summary, Ct (**1t**) is transformed into compound **5** by two

[2] Freshly prepared solutions were used to minimize the slow reactivity of the **Ct** species.

[3] The small variation reported at pH=6.2 in Fig. 3a was not observed in Fig. 4a because it occurs during the first stages of the reaction.

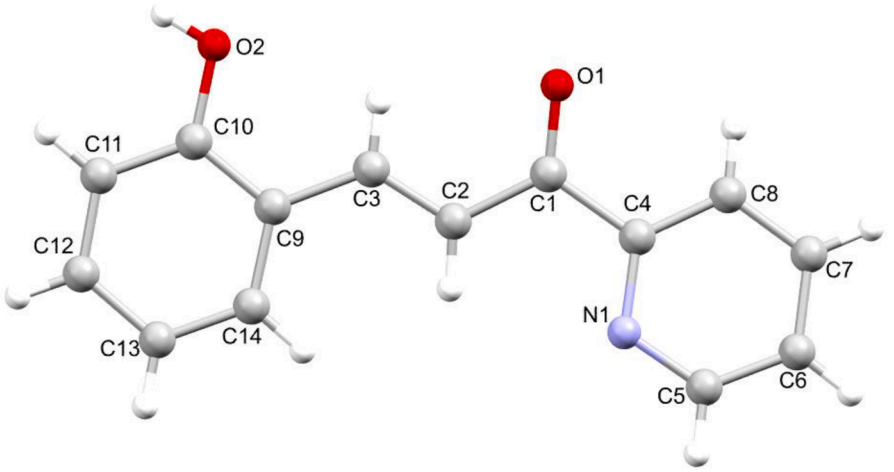

(a)

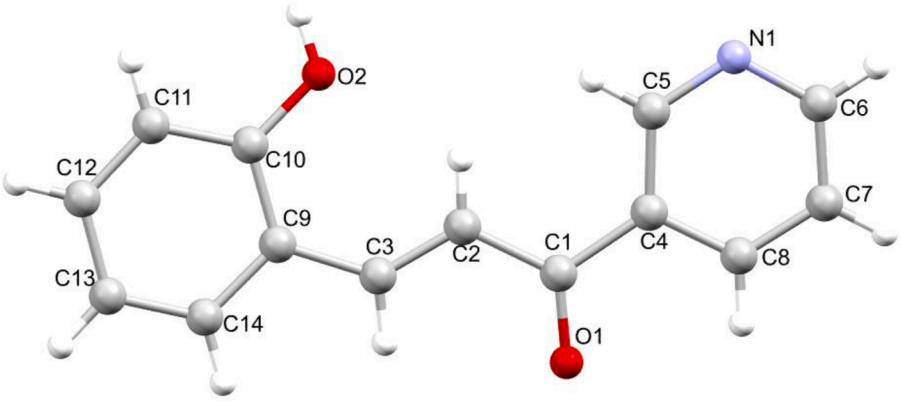

(b)

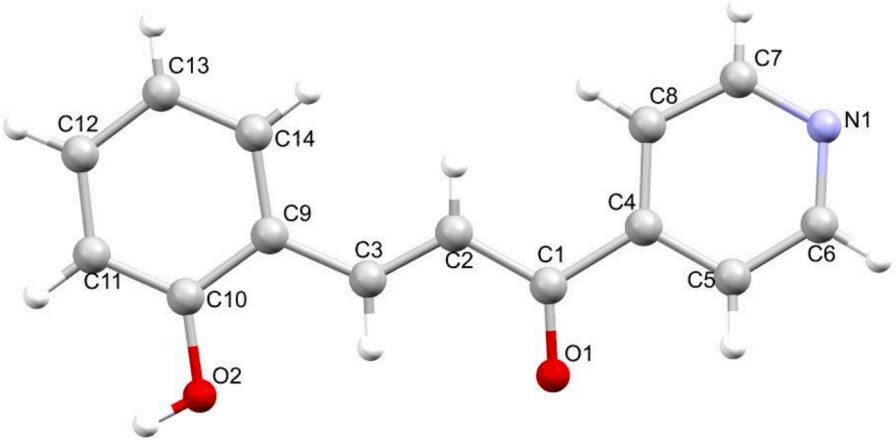

(c)

Fig. 12. Mercury drawings of the molecular structures of compounds (a) **Py2**, (b) **Py3** and (c) **Py4**.

Table 1
Selected bond lengths (Å) and angles (°) for compounds **Py2**, **Py3** and **Py4**.

	Py2	Py3	Py4
Distances (Å)			
C1–C2	1.4641(15)	1.462(6)	1.460(3)
C2–C3	1.3367(15)	1.327(5)	1.325(2)
C1–C4	1.4987(16)	1.485(5)	1.508(2)
C3–C9	1.4556(15)	1.437(5)	1.451(2)
C1–O1	1.2271(14)	1.226(4)	1.214(2)
Angles (°)			
C9–C3–C2	126.51(11)	131.7(4)	127.75(18)
C3–C2–C1	120.86(11)	123.4(4)	122.33(18)
C2–C1–C4	118.10(10)	119.6(5)	119.21(16)
C2–C1–O1	122.24(10)	121.6(5)	122.08(17)
C2–C1–C4–C8	168.39(11)	−178.1(3)	−7.1(3)
C2–C3–C9–C10	−176.77(11)	6.1(5)	−177.6(2)

Table 2
Crystal data and structure refinement for compounds **Py2**, **Py3** and **Py4**.

	Py2	Py3	Py4
Formula	$C_{14}H_{11}NO_2$	$C_{14}H_{11}NO_2$	$C_{14}H_{11}NO_2$
M	225.24	225.24	225.24
λ (Å)	0.71073	1.54178	0.71073
T (K)	296(2)	296(2)	293(2)
crystal system	Monoclinic	Monoclinic	Monoclinic
space group	$P2_1/n$	$P2_1/c$	$P2_1/n$
a (Å)	6.3345(2)	10.3400(5)	6.4171(3)
b (Å)	12.5688(5)	9.0867(4)	14.5107(6)
c (Å)	14.0305(6)	11.9877(5)	12.0942(5)
α (deg)	90	90	90
β (deg)	91.2740(10)	103.412(3)	94.308(2)
γ (deg)	90	90	90
V (Å^3)	1116.79(7)	1095.60(9)	1122.99(8)
Z	4	4	4
ρ_{calc} (g cm^{-3})	1.340	1.366	1.332
μ (mm^{-1})	0.090	0.747	0.090
θ_{max} (deg)	32.031	36.378	25.660
total data	40,355	4459	23,778
unique data	3865	522	2116
R_{int}	0.0544	0.0331	0.0682
R [*I* greater than 3σ(*I*)]	0.0563	0.0295	0.0542
wR_2	0.1486	0.0775	0.1442
Goodness of fit	1.069	1.062	0.935
ρ min ρ max	−0.195	−0.077	−0.221
	0.334	0.118	0.172

different mechanisms depending on the pH. For neutral pH values, Ct is directly transformed into compound **5**, while for acidic pH values where the pyridine is protonated, this transformation occurs *via* compound **4** (Scheme 8).

3.1.2. Photochemistry (water:methanol (1:1))

The spectral variations upon irradiation at 365 nm of freshly prepared solutions of the compound **Py2** are shown in Fig. 6. Short irradiation times were used to avoid the photochemical reactions of the primary photochemical products obtained from **1t**. The scope of this experiment is to assess the dark reactions that take place upon overcoming the strong *cis–trans* isomerization barrier, which is not possible from the thermal evolution at pH = 6. HPLC was used to follow these reactions that occur in the dark, Fig. 7.

When the thermal evolution of neutral solutions (Fig. 4a) is compared with the dark evolution in the dark after irradiation (Fig. 7a), the most significant difference is the formation of a broad peak attributed to the hemiketal, peak 3, which evolves to the expected mixture of **1t** and **5**. Compound **4** is again not detected at neutral pH values. Identical comparison in acid medium (Fig. 4b and Fig. 7b) shows that after 15 min of irradiation the mole fraction of chalcones and hemiketal are very small and compound **4** is the main species. As expected, the evolution in the dark corresponds to the slow transformation of compound **4** to compound **5**.

The thermal recovery of the photochemical products was also followed by UV–vis absorption, Fig. 8, and the data obtained is in accordance with the observations from by HPLC (Fig. 7). At pH = 6.2 (Fig. 8a), the *trans*-chalcone (**1t**) thermal recovery competes with the formation of compound **5**. In acidic medium, it is clear the formation of the absorption spectra attributed to compound **4** after 10 h (see above Fig. 11a) and the one of compound **5** after 61 h (compare with Fig. 11b).

3.1.3. The effect of the solvent

The photochemical reaction of *trans*-chalcone **1t** in CD_3OD was monitored by ^{1}H NMR, Fig. 9. After 90 min irradiation at 365 nm the *trans*-chalcone (**1t**, r.t. = 27.0 min) completely disappears to give a mixture of *cis*-chalcone (**1c**, r.t. = 29.1 min) and hemiketal (**3**, r.t. = 22.5 min). This solution evolves in the dark to the final product that was identified by ^{1}H NMR as hemiketal, Fig. 9a (see supplementary material for the assignment). The HPLC data, Fig. 9b, corroborates the ^{1}H NMR data, and allows to obtain the absorption spectrum of pure hemiketal, see Fig. 11b.

In order to study the effect of water in the multistate, addition of 20

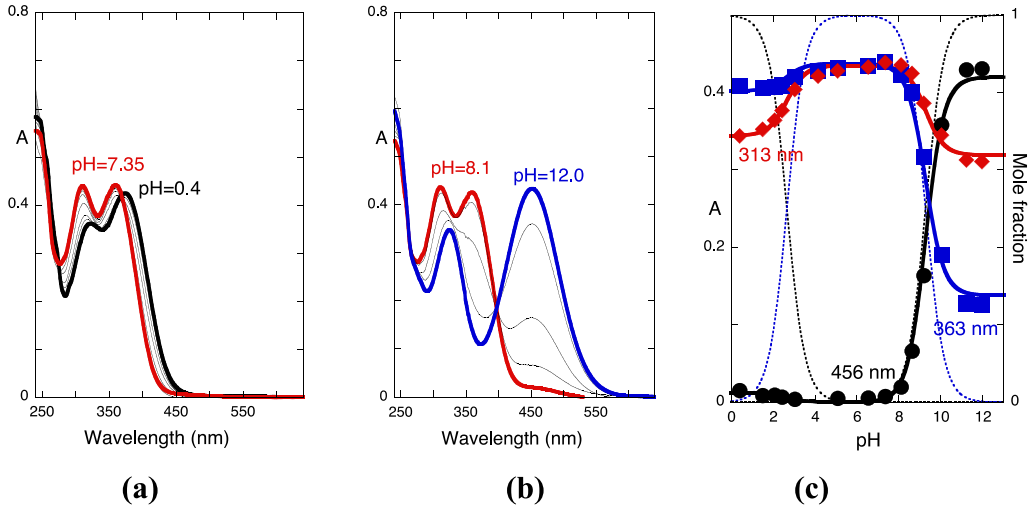

Fig. A1. Spectral variations of freshly prepared solutions of compound **Py3** 1.2×10^{-4} M in water:methanol (1:1) taken immediately after the pH jumps to 0.4 < pH < 7.35 **(a)** and to 8.1 < pH < 12.0 **(b)**, and respective titration curves **(c)**. Fitting was achieved for $pK_{Ct+/Ct} = 2.7$ and $pK_{Ct/Ct-}$=9.3.

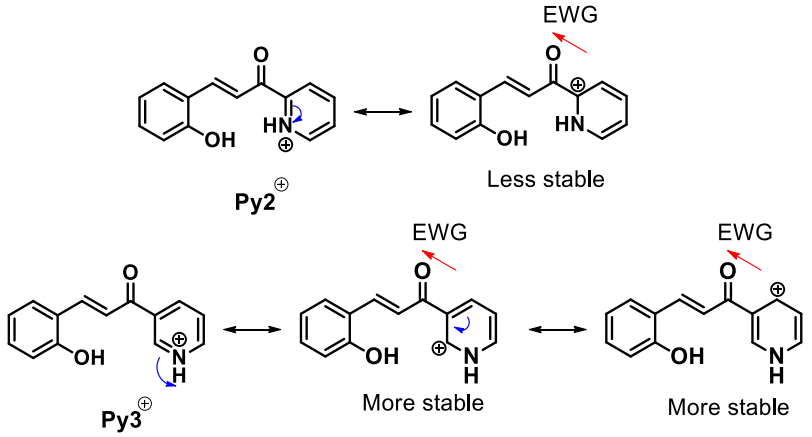

Scheme A1. Stabilization of the positive charge on protonated **Py2** and **Py3**. EWG: Electron withdrawing group.

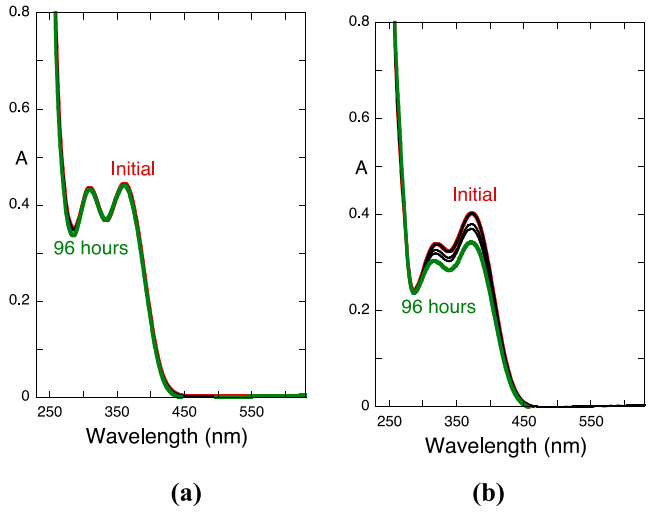

Fig. A2. Spectral variations of the compound **Py3** 1.2 × 10^{-4} M in water: methanol (1:1) after 96 h at pH = 6.5 **(a)** and at pH = 1.5 **(b)**.

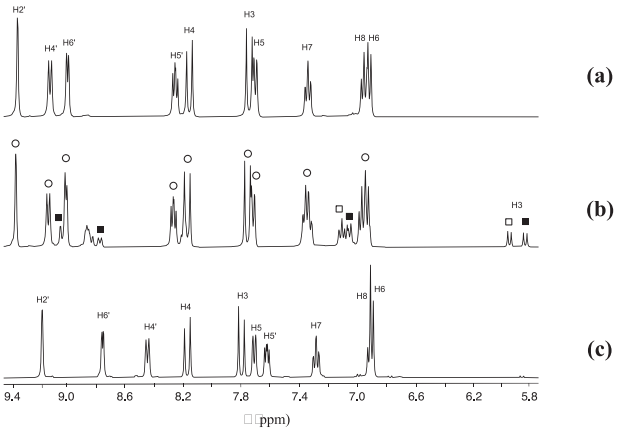

Fig. A3. ^{1}H NMR spectra (400 MHz, 300 k, CD_3OD/D_2O 1:1) of **Py3** 1.7 × 10^{-2} M. **(a)** immediately after a pH jump from pD = 6.6 to pD = 1.0, 100% of Ct^{+}; **(b)** the same solution of (a) dark equilibrated after 5 days, 14.5% Cc^{+} (□); 14.5% B^{+} (■); 71% Ct^{+} (○); **(c)** solution at pD = 6.6, Ct (purity more than 95%).

μL of DCl (12 M) to the solution obtained at the end of the experience reported in Fig. 9-III (and also shown in Fig. 10a-I) leads to the protonated hemiketal, Fig. 10a-II. Addition of D_2O to get a final solution with methanol:water (1:1) gives, after 48 h, a mixture of products where the major compound is assigned to compound **4** by HPLC (Fig. 10b-V).

In Fig. 11 the absorption spectrum of compound **4** is shown. When this spectrum is compared with the one of Fig. 6b it is clear that they are identical in the visible region allowing to conclude that one of the major products obtained upon the photochemical reaction in acidic medium is the compound identified as **4**.

Summarizing, **Py2** can add two new compounds to the respective multistate, underlining the importance of position 2 to interact chemically with the chalcone moiety (Scheme 9). The formation of these two new peaks depends on the water concentration, which plays an important role in the stabilization of both species.

Conversely, in the case of **Py3** and **Py4** the system is stable. The data regarding **Py3** is presented and discussed in the Appendix.

3.2. *X-ray diffraction studies*

Compounds **Py2**, **Py3** and **Py4** were crystallized from MeOH, MeOH: Et_2O (2:1) and MeOH:Et_2O (1:1), respectively, as green (**Py2**) and yellow (**Py3** and **Py4**) plates, suitable for single-crystal X-ray diffraction, with their molecular structures being unambiguously established by X-ray diffraction. A Mercury diagram of the asymmetric units is depicted in Fig. 12, the most significant bond distances and angles being given in the Table 1.

All compounds crystallized in the monoclinic system, with **Py2** and **Py4** in the $P2_1/n$ space group, whereas $P21/c$ space group was observed for **Py3**, showing only one molecule in the asymmetric unit. Although the synthesis of compound **Py4** was reported in our earlier communication, [27] no reports on its molecular structure were found and, therefore, it was also included in this paper for structural comparison with derivatives **Py2** and **Py3**. All molecular structures consist of the (*E*) isomers of prop-2-en-1-one, containing as substituents 1-pyridinyl derivatives, namely 1-(pyridin-2-yl), 1-(pyridin-3-yl) or 1-(pyridin-4-yl), for **Py2**, **Py3** and **Py4**, respectively, and 3-(2-hydroxyphenyl) moieties. All distances and angles in the three isomers are very similar (Table 1) and are within the expected values for similar compounds. [37] All compounds are nearly planar, displaying dihedral angles between the two aromatic rings of 7.69(4)°, 5.43(19)°, and 7.56(7)°, for **Py2**, **Py3** and **Py4**, respectively. Nevertheless, despite the small differences, **Py3** shows the smaller dihedral angle, being the most planar derivative.

In all isomers, **Py2**, **Py3** and **Py4**, classic O–H···O and O–H···N hydrogen bonds, and C–H···O and C–H···N assisted non-classical hydrogen bonds generate infinite 1D-chains, as depicted in Figures S21–S23 and Table S8 (see Supporting Information). Due to the

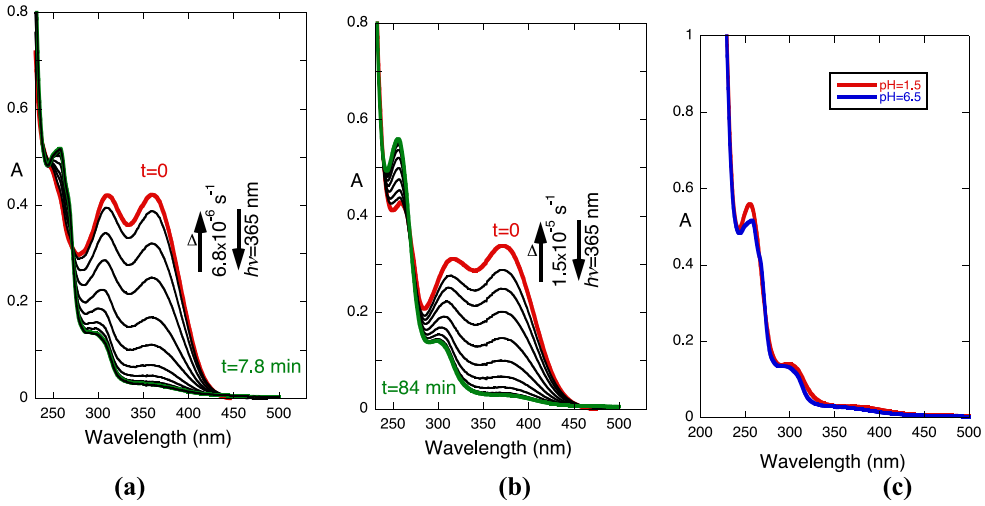

Fig. A4. **(a)** Irradiation of the compound **Py3**, 1.2 $\times$ 10^{-4} M in methanol:water (1:1) at 365 nm and pH = 6.5; **(b)** the same at pH = 1.5; **(c)** Comparison between the two photostationary states.

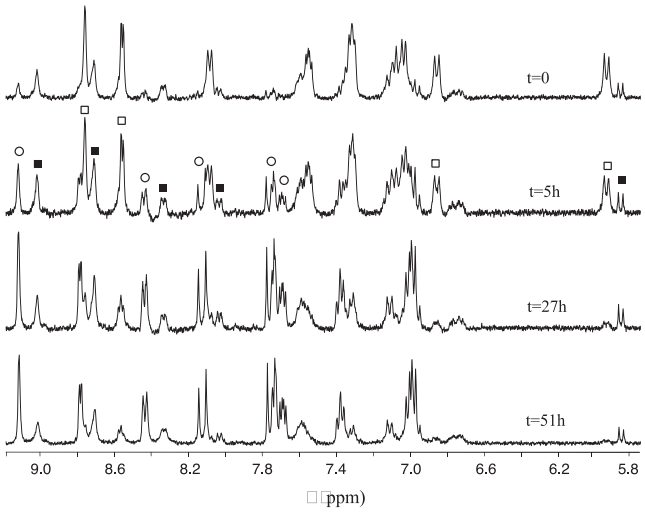

Fig. A5. Recovery of thermal reaction by ^{1}H NMR of **Py3** 1.7 $\times$ 10^{-2} M in CD_3OD/D_2O (1:1 v/v) at pD = 6.95; initial spectrum after 1 h of continuous irradiation at 365 nm B (■), Cc (□) e Ct (○).

supramolecular interactions described above, the crystal packing of **Py2** and **Py4** show zigzag arrangements when viewed along *a*, whereas **Py3** shows a continuous T-shaped arrangement when viewed along the *c* axis, as depicted in Figures S24–S26 (see Supporting Information).

4. Conclusions

The complex multistate of species observed in anthocyanins is followed by many other compounds including those where ring B is a pyridine. What is common in this last family is the lack of flavylium cation formation due to protonation of the nitrogen atom in the pyridine ring. However, the position of the nitrogen atom at the B ring is crucial for the reactivity of the multistate. In fact, a nitrogen atom at position 3′ or 4′ of pyridinechalcones allows to reach a common multistate of species in which the expected compounds B, Cc and Ct are present. However, if the nitrogen atom is at position 2′, two new species appear on the multistate, compound **4** and compound **5**, reported here for the first time. The presence of water is indispensable to promote the formation of these compounds. This fact opens the possibility of exploring a new family of compounds bio-inspired in anthocyanins with potential applications in the design of new photochromic systems and as biological active compounds.

Moreover, and due to the slow interconversion kinetics observed for this multistate of species, the inclusion of ^{1}H NMR, and HPLC-MS techniques along with the traditional UV–vis spectroscopy, allows reaching a rather deep understanding of the behaviour of these systems.

CRediT authorship contribution statement

Ambrósio Camuenho: Writing – review & editing, Writing – original draft, Methodology, Investigation, Formal analysis. **A. Jorge Parola:** . **Alfonso Alejo-Armijo:** Writing – review & editing, Writing – original draft, Supervision, Methodology, Investigation, Formal analysis. **Clara S.B. Gomes:** Writing – review & editing, Methodology, Investigation, Formal analysis. **César A.T. Laia:** Writing – original draft, Methodology. **Fernando Pina:** Writing – review & editing, Writing – original draft, Methodology, Formal analysis, Conceptualization.

Declaration of Competing Interest

The authors declare that they have no known competing financial interests or personal relationships that could have appeared to influence the work reported in this paper.

Data availability

Data will be made available on request.

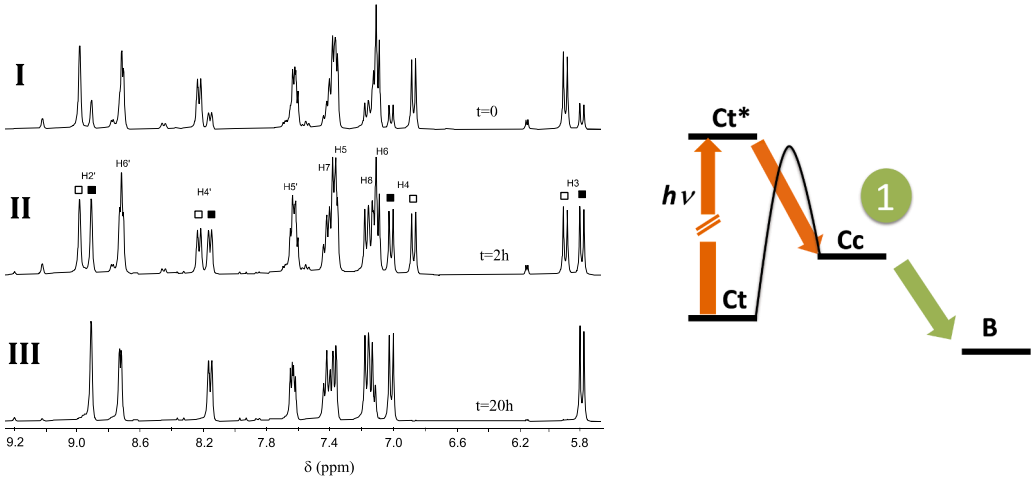

Fig. A6. **(a)** ^{1}H NMR of **Py3** 1.7×10^{-2} M in CD_3OD. I After irradiation at 365nm during 2h 75% Cc(□) and 25% B (■); II after dark equilibration 2h 50% Cc(□) and 50% B (■); III after 20h 100% B (■). The spectrum does not change after 5 days upon addition of DCl (final acid concentration 0.48M). **(b)** Qualitative energy diagram of **Py3** in CD_3OD.

Acknowledgements

This work was supported by the Associate Laboratory for Green Chemistry – LAQV (projects UIDB/50006/2020 and UIDP/ 50006/ 2020), the Research Unit on Applied Molecular Biosciences – UCIBIO (projects UIDP/04378/2020 and UIDB/ 04378/2020) and the Associate Laboratory Institute for Health and Bioeconomy – i4HB (project LA/P/ 0140/2020) which are financed by national funds from FCT/MCTES. FCT/MCTES is also acknowledged for supporting the National Portuguese NMR Network (ROTEIRO/0031/2013–PINFRA/22161/2016, cofinanced by FEDER through COMPETE 2020, POCI, PORL, and FCT through PIDDAC). A. C. acknowledges financing from Fundação Calouste Gulbenkian, grant no. 219201, and from the Angolan Embassy in Lisbon, Portugal, INAGBE grant. Dr. Ramesh Pandian is acknowledged for the initial acquisition and processing of single crystal X-ray data.

Appendix A

Py3 multistate

Fig. A1 shows the pH dependence of the absorption spectra of the compound **Py3** taken immediately after direct pH jumps from freshly prepared solutions of the *trans*-chalcone at pH = 6.6. The shape and position of the absorption spectra of Ct^+, Ct and Ct^- are similar to the parent **Py2**. The titration curves allow to calculate the following acidity constants, $pK_{a1} = 2.7$ and $pK_{a1} = 9.3$.

The second acidity constant corresponding to the deprotonation of the hydroxyl in **Py2** (Fig. 1 main text) and **Py3** are similar within the experimental error, but protonation of the pyridine ring is easier in **Py3**, due to the most favourable delocalization of the positive charge on the pyridine ring (Scheme A1).

The thermal stability of **Py3** is shown in Fig. A2. The absorption spectrum of Ct after 4 days does not show any modification at neutral pH (Fig. A2-a). At pH = 1.5 the protonated *trans*-chalcone Ct^+ presents a decreasing of its absorption after 4 days, but the spectral variations are not much informative (Fig. A2-b).

More information regarding this process was achieved by ^{1}H NMR, Fig. A3.

The ^{1}H NMR spectra of Fig. A3 confirms the stability of the species Ct at pD = 6.6. At acidic pD values an equilibrium is reached between protonated hemiketal, protonated *cis*-chalcone and protonated *trans*-chalcone after 5 days. Similarly to **Py2**, no flavylium cation was detected at this pD value.

The photochemistry of **Py3** was also explored and the respective spectral variations are shown in Fig. A4, for the species Ct^+ and Ct. It is worth of note the fact that the spectrum after 84 min at pH = 1.5 is more or less coincident with the one at pH = 6.5 (Fig. A4-c). Whatever are these species at the end of the irradiation process they are not protonated. This is different from the Ct species that due to its $pK_a = 2.7$ (Fig. A1) is expected to be protonated at pH = 1.5.

More information regarding the system was achieved following the thermal recovery by ^{1}H NMR, Fig. A5.

As expected, the irradiation of Ct gives Cc. This last species has two competitive pathways to evolve, which are dependent on the relative value of the respective rate constants: *i*) give back Ct, *ii*) give B in a transient way, because B tends to give back Ct (the thermodynamic species via Cc).

The same irradiation experiment was performed in MeOD 100% and the thermal recovery was followed ^{1}H NMR. This process is much more simple than in a mixture water:methanol. The thermal recovery after 2 h of irradiation of Ct at 365 nm is shown in Fig. A6.

Irradiation of **Py3** in MeOH allows to easily overcome the *cis–trans* isomerization barrier and allow the system to reach B species which is the most stable thermodynamic product in MeOH. The addition of D_2O to the system to have a solution with methanol:water 1:1, acid concentration 0.48 M recovers the *trans*-chalcone. It is expected that the non-classical tautomerization that occurs between B and Cc is favored in presence of water due to the stabilization of ionic intermediates.

Conjugation of the absorption and ^{1}H NMR data of Fig. S4 and Fig. S5 allows to conclude that, as expected, the primary product of the photochemical reaction is Cc that slowly evolves to the final state constituted by B.

Appendix B. Supplementary data

Supplementary data to this article can be found online at https://doi.org/10.1016/j.jphotochem.2023.114658.

References

[1] G.A. Iacobucci, J.G. Sweeny, The chemistry of anthocyanins, anthocyanidins and related flavylium salts, Tetrahedron 39 (19) (1983) 3005–3038, https://doi.org/10.1016/S0040-4020(01)91542-X.

[2] A. Castañeda-Ovando, M.d.L. Pacheco-Hernández, M.E. Páez-Hernández, J. A. Rodríguez, C.A. Galán-Vidal, Chemical studies of anthocyanins: a review, Food Chem. 113 (4) (2009) 859–871.

[3] J. Oliveira, N. Mateus, V. De Freitas, Wine-inspired chemistry: anthocyanin transformations for a portfolio of natural colors, Synlett 28 (8) (2017) 898–906, https://doi.org/10.1055/s-0036-1589937.

[4] F.H. Quina, E.L. Bastos, Chemistry inspired by the colors of fruits, flowers and wine, An. Acad. Bras. Cienc. 90 (1) (2018) 681–695, https://doi.org/10.1590/0001-3765201820170492.

[5] L. Cruz, N. Basílio, N. Mateus, V. de Freitas, F. Pina, Natural and synthetic flavylium-based dyes: the chemistry behind the color, Chem. Rev. 122 (1) (2022) 1416–1481, https://doi.org/10.1021/acs.chemrev.1c00399.

[6] F. Pina, M.J. Melo, C.A.T. Laia, A.J. Parola, J.C. Lima, Chemistry and applications of flavylium compounds: a handful of colours, Chem. Soc. Rev. 41 (2) (2012) 869–908, https://doi.org/10.1039/C1CS15126F.

[7] M.J. Melo, S. Moura, A. Roque, M. Maestri, F. Pina, Photochemistry of luteolinidin, J. Photochem. Photobiol. A Chem. 135 (1) (2000) 33–39, https://doi.org/10.1016/S1010-6030(00)00272-0.

[8] A. Alejo-Armijo, A.J. Parola, F. Pina, PH-dependent multistate system generated by a synthetic furanoflavylium compound: an ancestor of the anthocyanin multistate of chemical species, ACS Omega 4 (2) (2019) 4091–4100, https://doi.org/10.1021/acsomega.8b03696.

[9] A. Alejo-Armijo, J. Mendoza, A.J. Parola, F. Pina, Chemical evolution of the colour systems generated by riccionidin A, 3-deoxyanthocyanidins and anthocyanins, Phytochemistry 174 (March) (2020), 112339, https://doi.org/10.1016/j.phytochem.2020.112339.

[10] R. Gavara, V. Petrov, F. Pina, Characterization of the 4′-Hydroxynaphthoflavylium network of chemical reactions, Photochem. Photobiol. Sci. 9 (3) (2010) 298–303, https://doi.org/10.1039/b9 pp00035f.

[11] A. Alejo-Armijo, L. Corici, L. Cseh, D. Aparaschivei, A.J. Moro, A.J. Parola, J. C. Lima, F. Pina, Achieving complexity at the bottom. 2,6-bis(arylidene)cyclohexanones and anthocyanins: the same general multistate of species, ACS Omega 3 (12) (2018) 17853–17862.

[12] A. Alejo-Armijo, A.J. Moro, A.J. Parola, J.C. Lima, F. Pina, L. Corici, S. Shova, L. Cseh, Generalization of the anthocyanins kinetics and thermodynamics multistate to 2,6-bis(2-hydroxybenzylidene)cyclohexanones, Dye. Pigment. 163 (2019) 573–588.

[13] S. Slavcheva, J. Mendoza, S. Stanimirov, I. Petkov, N. Basílio, F. Pina, V. Petrov, On the multistate of 2′-hydroxyflavylium-flavanone system. Illustrating the concept of a timer with reset at the molecular level, Dye. Pigment. 158 (April) (2018) 465–473, https://doi.org/10.1016/j.dyepig.2018.05.066.

[14] P. Figueiredo, J.C. Lima, H. Santos, M. Wigand, R. Brouillard, A.L. Maqanita, F. Pina, Q. Base, Photochromism of the synthetic 4',7-dihydroflavylium chloride, J. Am. Chem. Soc. 116 (1994) 1249–1254.

[15] F. Pina, V. Petrov, C.A.T. Laia, Photochromism of flavylium systems. An overview of a versatile multistate system, Dye. Pigment. 92 (2) (2012) 877–889, https://doi.org/10.1016/j.dyepig.2011.03.033.

[16] H. Wünscher, G. Haucke, P. Czerney, U. Kurzer, Photochromic properties of hydrolyzed benzopyrylium salts - the influence of substituents, J. Photochem. Photobiol. A Chem. 151 (1–3) (2002) 75–82, https://doi.org/10.1016/S1010-6030(02)00017-5.

[17] R. Matsushima, M. Suzuki, Photochromic properties of 2-hydroxychalcones in solution and polymers, Bull. Chem. Soc. Jpn. 65 (1) (1992) 39–45, https://doi.org/10.1246/bcsj.65.39.

[18] F. Pina, M.J. Melo, M. Maestri, R. Ballardini, V. Balzani, Photochromism of 4'-methoxyflavylium perchlorate. A "Write−Lock−Read−Unlock−Erase" molecular switching system, J. Am. Chem. Soc. 119 (24) (1997) 5556–5561, https://doi.org/10.1021/ja9704646.

[19] H. Horiuchi, H. Shirase, T. Okutsu, R. Matsushima, H. Hiratsuka, Photochromism of 2-hydroxy-4′-methoxychalcone: A novel photon-mode erasable optical memory system with nondestructive readout ability, Chem. Lett. 2 (2000) 96–97, https://doi.org/10.1246/cl.2000.96.

[20] D. Costa, A.M. Galvão, R.E. Di Paolo, A.A. Freitas, J.C. Lima, F.H. Quina, A. L. Maçanita, Photochemistry of the hemiketal form of anthocyanins and its potential role in plant protection from UV-B radiation, Tetrahedron 71 (20) (2015) 3157–3162, https://doi.org/10.1016/j.tet.2014.06.092.

[21] M. Kondoh, A. Sakuta, K. Okazawa, D. Akase, M. Aida, T.-A. Ishibashi, Photo-Induced Ring-Opening Reaction of Flav-3-en-2-ol Monitored by Time-Resolved Infrared Spectroscopy, J. Phys. Chem. B 123 (40) (2019) 8499–8504, https://doi.org/10.1021/acs.jpcb.9b07108.

[22] S. Gago, N. Basílio, A.J. Moro, F. Pina, Flavylium based dual photochromism: addressing cis - trans isomerization and ring opening-closure by different light inputs, Chem. Commun. 51 (34) (2015) 7349–7351, https://doi.org/10.1039/c5cc01677k.

[23] V.O. Silva, A.A. Freitas, A.L. Maçanita, F.H. Quina, Chemistry and photochemistry of natural plant pigments: the anthocyanins, J. Phys. Org. Chem. 29 (11) (2016) 594–599, https://doi.org/10.1002/poc.3534.

[24] N. Basílio, F. Pina, Chemistry and photochemistry of anthocyanins and related compounds: a thermodynamic and kinetic approach, Molecules 21 (11) (2016), https://doi.org/10.3390/molecules21111502.

[25] F. Pina, M.J. Melo, A.J. Parola, M. Maestri, V. Balzani, PH-controlled photochromism of hydroxyflavylium ions, Chem. - A Eur. J. 4 (10) (1998), https://doi.org/10.1002/(SICI)1521-3765(19981002)4:10<2001::AID-CHEM2001>3.0.CO;2-P.

[26] F. Pina, A. Roque, M.J. Melo, M. Maestri, L. Belladelli, V. Balzani, Multistate/multifunctional molecular-level systems: light and ph switching between the various forms of a synthetic flavylium salt, Chem. - A Eur. J. 4 (7) (1998) 1184–1191, https://doi.org/10.1002/(SICI)1521-3765(19980710)4:7<1184::AID-CHEM1184>3.0.CO;2-6.

[27] Y. Leydet, A.J. Parola, F. Pina, Hydroxypyridinechromene and pyridinechalcone: two coupled photochromic systems, Chem. Eur. J. 16 (2) (2010) 545–555, https://doi.org/10.1002/chem.200901884.

[28] R. Gomes, A.J. Parola, C.A.T. Laia, F. Pina, Promoting photochromism on flavylium derived 2-hydroxychalcones in aqueous solutions by addition of CTAB micelles, J. Phys. Chem. B 111 (42) (2007) 12059–12065, https://doi.org/10.1021/jp073859c.

[29] R. Gomes, A.J. Parola, C.A.T. Laia, F. Pina, Efficient photochromism from the network of chemical reactions of 7,4′-dihydroxyflavylium in CTAB micelles, Photochem. Photobiol. Sci. 6 (9) (2007) 1003–1009.

[30] F.W. Küster, A. Thiel, Tabelle per Le Analisi Chimiche e Chimico-Fisiche, Hoepli (1999).

[31] A. Camuenho, A.J. Parola, A. Alejo-Armijo, R. Pandian, C.S.B. Gomes, C.A.T. Laia, F. Pina, A Model Compound for Pyridinechalcone-Based Multistate Systems. Ring Opening-Closure as the Slowest Kinetic Step of the Multistate, New J. Chem. 43 (46) (2019) 18229–18239, https://doi.org/10.1039/c9nj04776j.

[32] G.M. Sheldrick, Crystal Structure Refinement with SHELXL, Acta Crystallogr. Sect. C Struct. Chem. 71 (1) (2015) 3–8, https://doi.org/10.1107/S2053229614024218.

[33] G.M. Sheldrick, A short history of SHELX, Acta Crystallogr. Sect. A Found. Crystallogr. 64 (1) (2008) 112–122, https://doi.org/10.1107/S0108767307043930.

[34] G.M. Sheldrick, SHELXS-97 and SHELXL-97, Program for Crystal Structure Solution and Refinement, University of Gottingen, Gottingen, 1997.

[35] L.J. Farrugia, WinGX and ORTEP for windows: An update, J. Appl. Crystallogr. 45 (4) (2012) 849–854, https://doi.org/10.1107/S0021889812029111.

[36] C.F. Macrae, I. Sovago, S.J. Cottrell, P.T.A. Galek, P. McCabe, E. Pidcock, M. Platings, G.P. Shields, J.S. Stevens, M. Towler, P.A. Wood, Mercury 4.0: from visualization to analysis, design and prediction, J. Appl. Crystallogr. 53 (1) (2020) 226–235, https://doi.org/10.1107/S1600576719014092.

[37] F.H. Allen, The Cambridge structural database: A quarter of a million crystal structures and rising, Acta Crystallogr. Sect. B Struct. Sci. 58 (3) (2002) 380–388, https://doi.org/10.1107/S0108768102003890.